ChemistryEurope
Excellence in Chemistry Research Worldwide

Research Article
doi.org/10.1002/ceur.202400023

www.journal.chemistry-europe.org

Direct 2,2,2-Trifluoro and 2,2-Difluoroethoxylation of a Model Macrocyclic Ar–H Substrate via Ni-Catalysis

Lorena Capdevila,[a] Max T. G. M. Derks,[b] Marc Montilla,[a] Josep M. Luis,*[a] Jana Roithová,*[b] and Xavi Ribas*[a]

Herein, we describe the trifluoro- and difluoroethoxylation of C(sp^2)-H bonds using nickel(II) complexes incorporating a model macrocyclic arene substrate. Due to the coordinative properties of the macrocyclic substrate, we were able to detect and characterize the just-formed C(sp^2)–OCH_2CF_3–Ni(II) species by HRMS and IRPD. DFT studies on the C(sp^2)–OCH_2CF_3 bond formation mechanism indicate that it involves a Ni(III)/Ni(I) reductive elimination followed by oxidation to Ni(II) rather than the higher energy barrier Ni(IV)/Ni(II) reductive elimination. This mechanistic investigation deepens the versatile redox abilities of Ni compounds and might help in designing new catalysts for the 2,2,2-trifluoroethoxylation and 2,2-difluoroethoxylation of arene C–H bonds.

Introduction

Aryl ethers are valuable compounds with widespread applications such as solvents, pharmaceuticals, and medicinal compounds.[1] Ethers are typically synthesized via Williamson ether synthesis, Buchwald-Hartwig couplings, or Ullmann reactions. These methods, however, suffer from various limitations such as the requirement of excess metal, multi-step synthesis, and the use of pre-functionalized starting materials.[2] On the other hand, catalytic cross-coupling reactions involving C-(sp^2)–O bond formation using aliphatic alcohols ($HOCH_2R$, R=H, CH_3, CF_3, etc.) have been explored using Cu(I)/Cu(III),[3] Ni(I)/Ni(III),[4] Ni(II)/Ni(IV),[5] and even in Au(I)/Au(III) catalysts as model systems.[6] Also, light-irradiated Ni-catalyzed C–O coupling has been developed (involving Ni(I)/Ni(III)/radical cycles).[7] On the contrary, selective direct functionalization of C–H bonds into C–O bonds remains a highly desirable but challenging transformation due to the harsher conditions commonly required.[8]

In synergy with the latter, the pharmaceutical industry actively seeks new methodologies for introducing fluorinated ether motifs. These motifs change the physical, chemical, and biological properties and may improve both the stability and lifetime of F-containing pharmaceuticals.[3,9] A metal-catalyzed fluoroalkoxylation of C(sp^2)–H via C–H activation may be key to developing such synthetic methodologies and may yield an improved synthetic pathway for targets such as antitachycardic Flecainide[10] and the stomachal antiacid Lansoprazole (Figure 1a).[11]

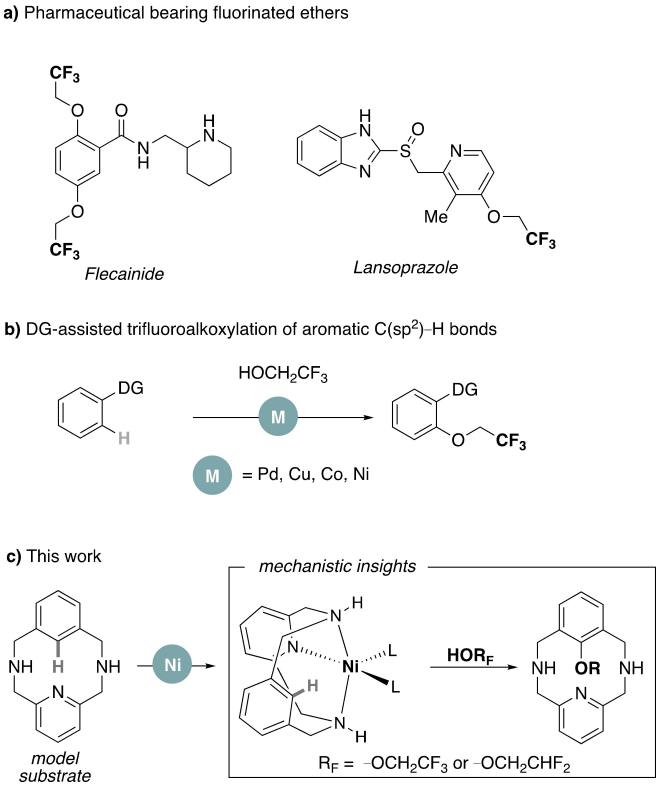

Figure 1. (a) Antitachycardic Flecainide and the stomachal antiacid Lansoprazole bearing the 2,2,2-trifluoroethoxy group. (b) TM-catalyzed trifluoroalkoxylation reaction by C(sp^2)–H activation. (c) Current mechanistic study on the Ni-based reactivity of a macrocyclic model substrate with fluorinated alcohols.

[a] L. Capdevila, M. Montilla, J. M. Luis, X. Ribas
Institut de Química Computacional i Catàlisi (IQCC)
and
Universitat de Girona, Maria Aurèlia Capmany, 69, Campus Montilivi, 17003 Girona, Catalonia, Spain
E-mail: josepm.luis@udg.edu
xavi.ribas@udg.edu

[b] M. T. G. M. Derks, J. Roithová
Department of Spectroscopy and Catalysis Institute for Molecules and Materials, Radboud University, Heyendaalsweg 135, 6525AJ Nijmegen, The Netherlands
E-mail: j.roithova@science.ru.nl

Supporting information for this article is available on the WWW under https://doi.org/10.1002/ceur.202400023

Research Article
doi.org/10.1002/ceur.202400023

The direct 2,2,2-trifluoroethoxylation of C(sp^2)–H using the 2,2,2-trifluoroethanol (TFE) as an inexpensive and green fluorinated source is manifestly underexplored.[2a,12] Pd-catalyzed dehydrogenative 2,2,2-trifluoroethoxylation of benzo[h]quinoline, reported by Sanford in 2004 was the first metal-catalyzed Ar-OCH_2CF_3 bond forming reaction via C–H activation.[13] Similar reactivity using 3-arylcoumarins was reported by Kumar recently.[14]

In the past decade, first-row transition metals have also been used for this transformation. Copper, cobalt, and nickel complexes allowed for the 2,2,2-trifluoroethoxylation of different substrates using a directing group (DG) strategy (Figure 1b). In 2013, Daugulis reported a Cu-catalyzed transformation using 3-trifluoromethylated benzamide derived from 8-aminoquinoline as substrate.[15] Furthermore, by the use of *N,N-* and *N,O-*bidentate directing groups, the construction of C(sp^2)–OCH_2CF_3 by C–H bond activation was also reported using Co-catalysis.[16] In the case of Ni-catalyzed examples, a unique example of an Ar–OCH_2CF_3 bond formation via C–H activation using TFE was reported by Sundararaju in 2018.[17] The 8-aminoquinoline directing group (DG) was key in the formation of the compound, although the catalysis had a low TON (~3).

In this context, we undertook a mechanistic study to better understand a 2,2,2-trifluoroethoxylation of Ar–H with a model macrocyclic substrate (**1**) (Figure 1c). The latter type of substrates has been used by our group to unravel numerous mechanistic insights disclosing otherwise inaccessible organometallic intermediates.[18]

Results and Discussion

The model arene-substrate **1** was used to synthesize the corresponding Ni(II) coordination compounds **2-OAc** and **2-ACN**, which were isolated and characterized, featuring the Ar–H bond still intact (Scheme 1). The solid-state molecular structure of **2-ACN** confirmed a pentacoordinated distorted-square-pyramidal geometry. Furthermore, the crystal structure shows incipient interactions between the Ni(II) and a hydrogen atom of the arene (Ni1···H12 distance of 2.37 Å and a Ni–C12–H12 angle of 73.6°. The structure of **2-OAc** was also confirmed by XRD analysis, where the Ni(II) center is coordinated to two acetates in a bidentate fashion and two N of the macrocycle ligand (through pyridine and one amine).

We explored the reactivity of both complexes (**2-OAc** and **2-ACN**) to different reaction conditions in TFE (CF_3CH_2OH) as solvent. Firstly, when the **2-ACN** complex was exposed to TFE in the presence of $FcPF_6$ as the oxidant and Cs_2CO_3 as the base, the trifluoroalcoxylated product (**P1**) was formed in 22% NMR yield after 1 hour (Figure 2a). The incorporation of the trifluoroethanoate molecule was also investigated using **2-OAc** complex. Under the same conditions, the **2-OAc** complex did not yield the **P1** product. Instead, we could detect new ions with *m/z* 454 by electrospray ionization mass spectrometry (ESI-MS).[19] The ions corresponded formally to the nickel complex $[(\mathbf{1}(-H))Ni(OAc)(OCH_2CF_3)]^+$. He-tagging infrared photodissociation (IRPD) spectroscopy helped elucidate the structure of this new complex.[20] Comparison of the experimental IRPD spectrum of the ions with *m/z* 454 with a spectrum of the most stable isomer corresponding to the isolated ions allowed us to identify the species as **5-OCH$_2$CF$_3$** (Figure 2b). The isomer corresponds to the C(sp^2)–O coupled product complex with nickel(II) in the triplet state, where the acetate is coordinated in a bidentate fashion. The **P1** product was formed by subjecting the crude mixture to acidic conditions in 31% NMR yield.

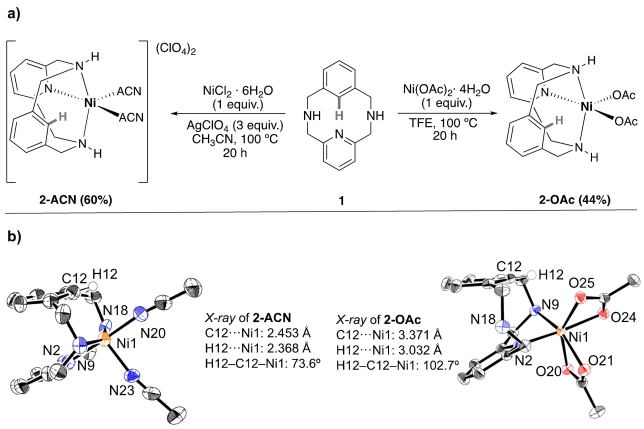

Scheme 1. (a) Synthesis of the Ni(II) complex **2-L**. (b) Crystal structures of **2-ACN** and **2-OAc** (Anions and H atoms have been omitted for clarity, except for inner aryl-H).

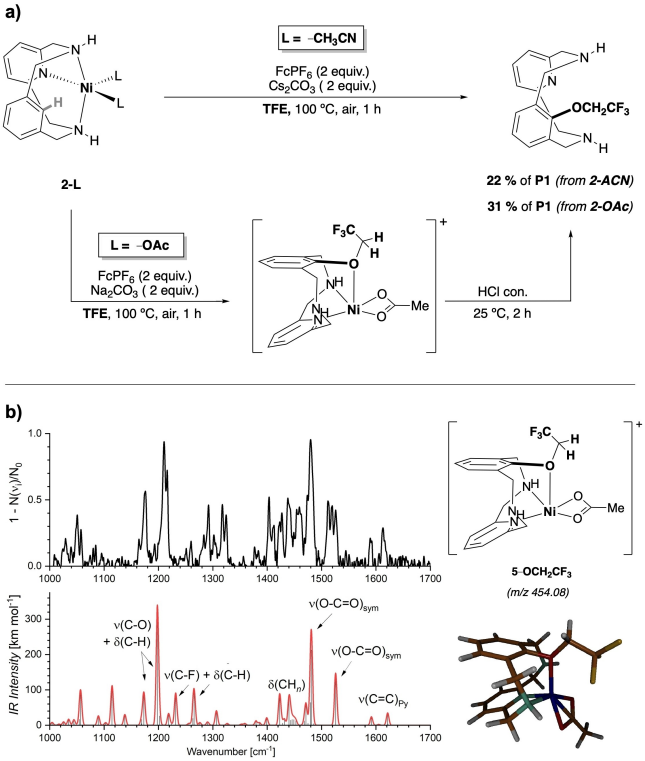

Figure 2. (a) Reactivity of **2-ACN** and **2-OAc** with TFE to afford **P1** product. (b) Comparison of the experimental IRPD spectrum with a spectrum of the most stable isomer of the product complex in the triplet ground state. The acetate is coordinated bidentally. For the comparison with IR spectra of other possible structures of the isolated ions, see Figures S31 and S32.

Research Article
doi.org/10.1002/ceur.202400023

The yield obtained for the stoichiometric reaction from **2-ACN** and **2-OAc** to afford the trifluoroethoxylated product **P1** is however low (22% and 31%, respectively). To improve the effectivity of the reaction, the optimization of the reaction under catalytic conditions (34 mol% **2-ACN**) afforded good results (Scheme 2), and 2 TON were obtained (57% NMR yield), indicating that the recovery of active Ni(II) at the end of the reaction cycle and its engagement to a subsequent catalytic cycle is possible. We then investigated the role of the nature of the fluorinated solvent. Interestingly, using difluoroethanol (DFE) and 40 mol% of **1-OAc** leads to the corresponding difluoroethoxylated product **P2** (52% NMR yield). Other fluorinated solvents, such as hexafluoro-2-propanol (HFIP) or trifluoropropanol, didn't afford the desired products, indicating that the acidity/nucleophilicity of the solvent is crucial for the reaction.

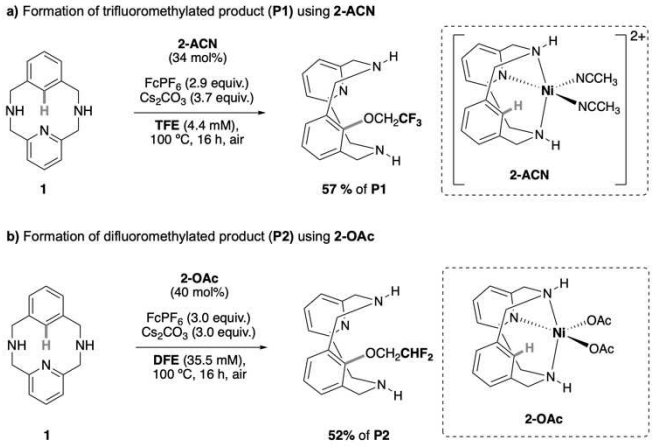

Scheme 2. Direct trifluoro- and difluoroethoxylation reactions using **2-ACN** or **2-OAc**.

As mentioned above, the species trapped by ESI-MS corresponds to **5-OCH$_2$CF$_3$**, which features the formation of the C(sp^2)–OCH$_2$CF$_3$ ethereal bond. Therefore, this valuable information points out that Ni(II) is the actual oxidation state at the end of the transformation.

However, no more information on the precise steps during the reaction can be extracted experimentally, and the oxidation state manifold remains unknown. Based on both the reactivity reported in literature and on the stability of the isolated Ni(II) complexes **2-OAc** and **2-ACN**, the proposed mechanism starts with the 1-electron oxidation by Fc$^+$ to Ni(III), which rapidly activates C–H bond of the substrate and forms the organometallic Ar–Ni(III) intermediates species (**3-L**) via a Concerted Metallation Deprotonation reaction (CMD) (Schemes 3 and 4).

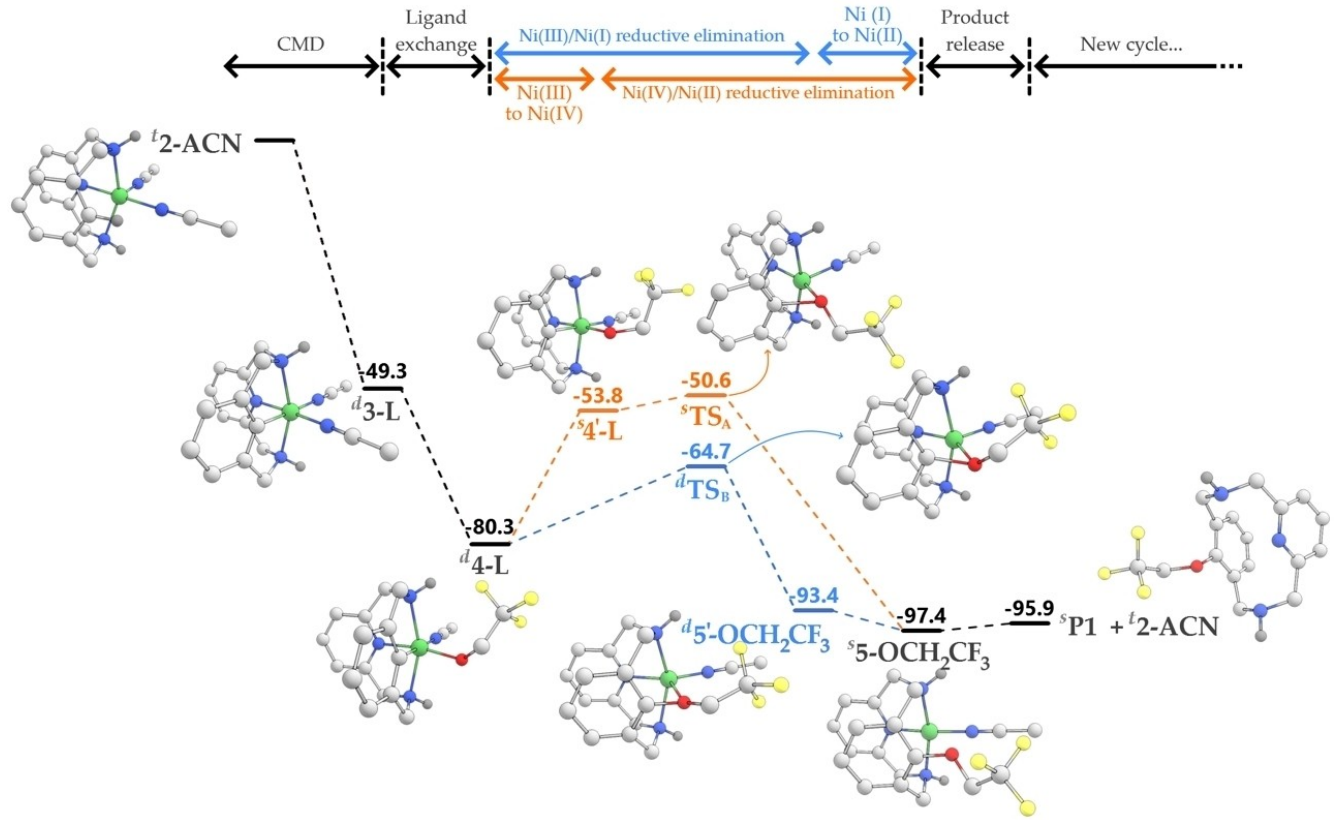

Scheme 3. Reaction Gibbs energy profile for the 2,2,2-trifluoroethoxylation of **2-ACN** computed at the MN15-D3BJ/Def2TZVP/SMD(TFE)//BP86-D3BJ/Def2SVP/SMD(TFE) level of theory. Gibbs energies are given in kcal·mol^{-1}. Superscripts s, d, and t represent spin states S = 0, S = 1/2, and S = 1, respectively. The blue pathway describes the Ni(III)/Ni(I) reductive elimination, and the orange pathway the Ni(IV)/Ni(II) reductive elimination. Geometries for all intermediates and transition states are shown (nitrogen atoms are represented in blue, oxygen in red, fluorine in yellow, nickel in green, carbon in white, and hydrogen in grey). For clarity, all hydrogens attached to carbon have been omitted (except for the inner aryl-H).

Research Article
doi.org/10.1002/ceur.202400023

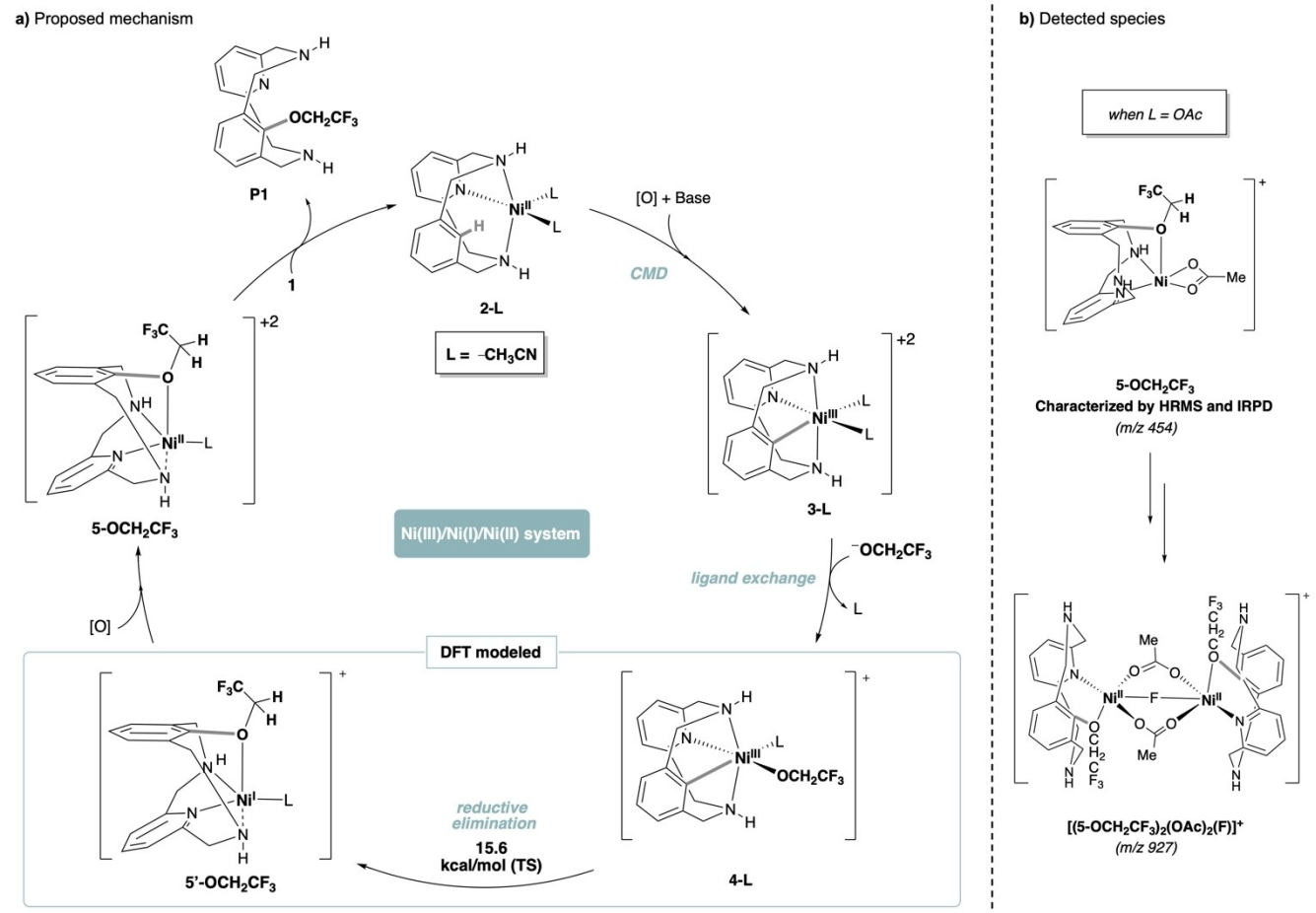

Scheme 4. (a) Proposed mechanism for the synthesis of **P1** using **2-ACN** complex. (b) Species detected by HRMS (**5-OCH_2CF_3** and $[(\mathbf{5\text{-}OCH_2CF_3})_2(AcO)_2(F)]^+$) and IRPD (**5-$OCH_2CF_3$**).

Under the basic conditions of the reaction, a ligand exchange allows the coordination of the 2,2,2-trifluoroethoxide to the Ni(III) center (Ar–Ni(III)–OCH_2CF_3, **4-L**). At this point, two different mechanisms can occur (Scheme 3): A) the Ar–Ni(III) species is further oxidized to Ni(IV) (**4′-L**), allowing the reductive elimination to form the Ar–OCH_2CF_3 product and Ni(II) (**5-OCH_2CF_3**); or B) the formed Ar–Ni(III)–OCH_2CF_3 directly undergoes reductive elimination to afford (Ar–OCH_2CF_3) and Ni(I) (**5′-OCH_2CF_3**), which is then reoxidized to Ni(II).

Both pathways would agree with observing the equivalent species to the experimentally detected **5-OCH_2CF_3**. To discern among the two possible pathways (A or B), we resorted to DFT studies at the MN15-D3BJ/Def2TZVP/SMD(TFE)//BP86-D3BJ/Def2SVP/SMD(TFE) level of the mechanism for the **2-ACN** catalyst (See SI for the computational details). The Concerted Metallation Deprotonation and ligand exchange steps are strongly exergonic (see SI for details), leading to the rapid formation of **4-L** from **2-ACN**. The calculated activation energy for the oxidation of Ar–Ni(III)–OCH_2CF_3 to Ar–Ni(IV)–OCH_2CF_3 by $FcPF_6$ followed by reductive elimination to Ni(II), was 29.7 kcal mol^{-1} (TS_A depicted in Scheme 3).

On the other hand, the calculated activation energy for the reductive elimination directly from Ar–Ni(III)–OCH_2CF_3 to (Ar–OCH_2CF_3)–Ni(I), afforded a barrier of 15.6 kcal mol^{-1} (TS_B depicted in Scheme 3). Subsequent exergonic oxidation to Ni(II) by $FcPF_6$ affords the **5-OCH_2CF_3** species. Finally, a slightly endergonic ligand exchange of the ethereal product **P1** by fresh substrate **1** renders a globally strongly exergonic process (−95.9 kcal/mol), ready to start a new catalytic cycle. The large energy difference of 14.1 kcal mol^{-1} between Ni(III)/Ni(I)/Ni(II) and Ni(III)/Ni(IV)/Ni(II) pathways confirms the former pathway as the more accessible and operating mechanism in this reaction. We further validated the studied Gibbs energy profile using wB97XD/Def2TZVP/SMD(TFE)//BP86-D3BJ/Def2SVP/SMD(TFE) and B3LYP-/Def2TZVP/SMD(TFE)//BP86-D3BJ/Def2SVP/SMD(TFE) levels, reaching the same conclusions (Figures S25 and S26). Additionally, DFT calculations indicate that a putative disproportionation of the Ni(III) species (**4-L**) into Ni(IV) and Ni(II) is energetically inaccessible (Table S5).

Moreover, the reaction is merely shut down when temperature is lowered below 60 °C (Table S1) and we couldn't detect the formation of the corresponding Ni(III) organometallic complex **3-L** (with two coordinated CH_3CN) or **4-L** (with one –CH_3CN and one –OCH_2CF_3). All these results suggest that the limiting step of the reaction is the activation of the C–H bond via CMD, with an estimated barrier of 26–28 kcal/mol. Cyclic

Research Article
doi.org/10.1002/ceur.202400023

Voltammetry (CV) analysis of **2-ACN** in TFE (Figure S33) also supports the irreversible oxidation by Fc^+ to Ni(III) to effect the CMD C–H activation.

Considering these data, our mechanistic proposal (Scheme 4) involves the initial oxidation of Ni(II) to Ni(III), followed by the CMD reaction and formation of **3-L** as the rate-limiting step. In turn, ligand exchange under basic conditions allows obtaining **4-L**. Subsequently, the latter undergoes reductive elimination to form Ni(I) **5′-OCH_2CF_3**, rapidly oxidizing to Ni(II) **5-OCH_2CF_3** under the employed reaction conditions. While performing the HRMS monitoring, a peak corresponding to a dimer of Ni(II) at m/z = 927 was observed, and the MS/MS analysis of this peak afforded again the 454 peak corresponding to **5-OCH_2CF_3**. The latter suggested that the ions with *m/z* 927 were a product of dimerization of **5-OCH_2CF_3**, tentatively assigned to $[(\mathbf{5\text{-}OCH_2CF_3})_2(AcO)_2(F)]^+$. The source of F^- is the decomposition under the MS conditions of the PF_6^- anion present in the oxidant ($FcPF_6$).

Since the ferrocenium scaffold can be chemically modified, different derivatives with tuned redox potentials can be accessed a priori. Our DFT calculations predict that an oxidant with a redox potential 0.6 V higher than Fc/Fc^+ could lower the Ni(III)/Ni(IV)/Ni(II) pathway to be competitive with the operating one (Figure S27). On the contrary, the reaction could still occur with a soft oxidant 0.3 V lower than Fc/Fc^+ (Figure S28).

Conclusions

In summary, we took advantage of the stabilization properties of the model arene-substrate **1** to synthesize the Ni(II) complexes **2-OAc** and **2-ACN**, and to expose them to different C–O bond-forming reaction conditions in TFE and DFE. The species trapped by MS coupled with He-tagging IRPD spectroscopy corresponds to **5-OCH_2CF_3**, which features the formation of the $C(sp^2)$–OCH_2CF_3 ethereal bond. Detecting this complex indicates that Ni(II) is the final oxidation state at the end of the transformation. Based on the stability of the isolated Ni(II) complexes **2-OAc** and **2-ACN** and other reactivity reported in the literature, a 1-e^- oxidation by Fc^+ to Ni(III) is proposed, which rapidly activates the arene $C(sp^2)$–H bond to form the intermediate Ar–Ni(III) (**3-L**) via CMD. A thorough DFT study allowed us to confidently propose the subsequent Ni(III)/Ni(I) reductive elimination from Ar–Ni(III)–OCH_2CF_3 (**4-L**) to (Ar–OCH_2CF_3)–Ni(I) (**5′-OCH_2CF_3**), followed by oxidation to Ni(II) (**5-OCH_2CF_3**). All this valuable mechanistic information might help in designing new Ni(I)/Ni(III) catalytic processes for the 2,2,2-trifluoroethoxylation and 2,2-difluoroethoxylation of arene C–H bonds.

Supporting Information

The authors have cited additional references within the Supporting Information.[21–29] Deposition Numbers CCDC 2334794 (**2-ACN**) and 2334793 (**2-OAc**) contain the supplementary crystallographic data for this paper.

Acknowledgements

This work was financially supported by grants from MINECO Spain (PID2022-136970NB-I00 to X.R. and PID2022-140666NB-C22 to JM.L), and Generalitat de Catalunya (2021SGR00475 and ICREA Academia to X.R.; 2021SGR00623 to JM.L). J.R. thanks to the Dutch Research Organization (NWO No. VI.C.192.044).

Conflict of Interests

The authors declare no conflict of interest.

Data Availability Statement

The data that support the findings of this study are available in the supplementary material of this article.

Keywords: Nickel organometallics · C–H activation · fluoroalkoxylation · Ni(I)/Ni(III) redox catalysis · He-tagging IRPD spectroscopy

[1] a) S. Enthaler, A. Company, *Chem. Soc. Rev.* **2011**, *40*, 4912–4924; b) S. D. Roughley, A. M. Jordan, *J. Med. Chem.* **2011**, *54*, 3451–3479.
[2] a) L. Monsigny, F. Doche, T. Besset, *Beilstein J. Org. Chem.* **2023**, *19*, 448–473; b) J. F. Hartwig, *Nature* **2008**, *455*, 314–322.
[3] L. M. Huffman, A. Casitas, M. Font, M. Canta, M. Costas, X. Ribas, S. S. Stahl, *Chem. Eur. J.* **2011**, *17*, 10643–10650.
[4] a) S. M. Smith, O. Planas, L. Gómez, N. P. Rath, X. Ribas, L. M. Mirica, *Chem. Sci.* **2019**, *10*, 10366–10372; b) K. M. Morrison, C. S. Yeung, M. Stradiotto, *Angew. Chem. Int. Ed.* **2023**, *62*, e202300686.
[5] C. Magallón, L. Griego, C. H. Hu, A. Company, X. Ribas, L. M. Mirica, *Inorg. Chem. Front.* **2022**, *9*, 1016–1022.
[6] J. Serra, T. Parella, X. Ribas, *Chem. Sci.* **2017**, *8*, 946–952.
[7] a) L. Yang, H.-H. Lu, C.-H. Lai, G. Li, W. Zhang, R. Cao, F. Liu, C. Wang, J. Xiao, D. Xue, *Angew. Chem. Int. Ed.* **2020**, *59*, 12714–12719; b) H. Na, L. M. Mirica, *Nat. Commun.* **2022**, *13*, 1313; c) J. Bahri, S. Deolka, P. K. Vardhanapu, E. Khaskin, R. Govindarajan, R. R. Fayzullin, S. Vasylevskyi, J. R. Khusnutdinova, *ChemCatChem* **2023**, *15*, e202301142.
[8] a) S. Bhadra, C. Matheis, D. Katayev, L. J. Gooßen, *Angew. Chem. Int. Ed.* **2013**, *52*, 9279–9283; b) L.-B. Zhang, X.-Q. Hao, S.-K. Zhang, K. Liu, B. Ren, J.-F. Gong, J.-L. Niu, M.-P. Song, *J. Org. Chem.* **2014**, *79*, 10399–10409.
[9] J. Wang, M. Sánchez-Roselló, J. L. Aceña, C. del Pozo, A. E. Sorochinsky, S. Fustero, V. A. Soloshonok, H. Liu, *Chem. Rev.* **2014**, *114*, 2432–2506.
[10] E. Paolini, G. Stronati, F. Guerra, A. Capucci, *Pharmacol. Res.* **2019**, *148*, 104443.
[11] A. J. Matheson, B. Jarvis, *Drugs* **2001**, *61*, 1801–1833.
[12] G. B. Kauffman, *Angew. Chem. Int. Ed.* **2008**, *47*, 8155–8156.
[13] A. R. Dick, K. L. Hull, M. S. Sanford, *J. Am. Chem. Soc.* **2004**, *126*, 2300–2301.
[14] V. N. Shinde, K. Rangan, D. Kumar, A. Kumar, *J. Org. Chem.* **2021**, *86*, 9755–9770.
[15] a) L. Grigorjeva, O. Daugulis, *Org. Lett.* **2014**, *16*, 4684–4687; b) J. Roane, O. Daugulis, *Org. Lett.* **2013**, *15*, 5842–5845.
[16] a) L.-B. Zhang, X.-Q. Hao, S.-K. Zhang, Z.-J. Liu, X.-X. Zheng, J.-F. Gong, J.-L. Niu, M.-P. Song, *Angew. Chem. Int. Ed.* **2015**, *54*, 272–275; b) S. Kumar, A. M. Nair, C. M. R. Volla, *Chem. Asian J.* **2022**, *17*, e202200801.
[17] N. Rajesh, B. Sundararaju, *Asian J. Org. Chem.* **2018**, *7*, 1368–1371.
[18] a) O. Planas, S. Roldán-Gómez, V. Martin-Diaconescu, J. M. Luis, A. Company, X. Ribas, *Chem. Sci.* **2018**, *9*, 5736–5746; b) O. Planas, S. Roldán-Gómez, V. Martin-Diaconescu, T. Parella, J. M. Luis, A. Company, X. Ribas, *J. Am. Chem. Soc.* **2017**, *139*, 14649–14655; c) O. Planas, C. J. Whiteoak, V. Martin-Diaconescu, I. Gamba, J. M. Luis, T. Parella, A. Company, X. Ribas, *J. Am. Chem. Soc.* **2016**, *138*, 14388–14397; d) X. Ribas, M. Devillard, *Chem. Eur. J.* **2018**, *24*, 1222–1230; e) C. Magallón, O.

Research Article
doi.org/10.1002/ceur.202400023

Planas, S. Roldán-Gómez, J. M. Luis, A. Company, X. Ribas, *Organometallics* **2021**, *40*, 1195–1200.
[19] J. Mehara, J. Roithová, *Chem. Sci.* **2020**, *11*, 11960–11972.
[20] a) J. Roithová, A. Gray, E. Andris, J. Jašík, D. Gerlich, *Acc. Chem. Res.* **2016**, *49*, 223–230; b) J. Roithova, *Chem. Soc. Rev.* **2012**, *41*, 547–559.
[21] a) O. Planas, C. J. Whiteoak, V. Martin-Diaconescu, I. Gamba, J. M. Luis, T. Parella, A. Company, X. Ribas, *J. Am. Chem. Soc.* **2016**, *138*, 14388–14397; b) O. Planas, S. Roldán-Gómez, V. Martin-Diaconescu, J. M. Luis, A. Company, X. Ribas, *Chem. Sci.* **2018**, *9*, 5736–5746; c) O. Planas, S. Roldán-Gómez, V. Martin-Diaconescu, T. Parella, J. M. Luis, A. Company, X. Ribas, *J. Am. Chem. Soc.* **2017**, *139*, 14649–14655.
[22] G. W. M. J. T. Frisch, H. B. Schlegel, G. E. Scuseria, M. A. Robb, J. R. Cheeseman, G. Scalmani, V. Barone, G. A. Petersson, H. Nakatsuji, X. Li, M. Caricato, A. V. Marenich, J. Bloino, B. G. Janesko, R. Gomperts, B. Mennucci, H. P. Hratchian, J. V. Ortiz, A. F. Izmaylov, J. L. Sonnenberg, D. Williams-Young, F. Ding, F. Lipparini, F. Egidi, J. Goings, B. Peng, A. Petrone, T. Henderson, D. Ranasinghe, V. G. Zakrzewski, J. Gao, N. Rega, G. Zheng, W. Liang, M. Hada, M. Ehara, K. Toyota, R. Fukuda, J. Hasegawa, M. Ishida, T. Nakajima, Y. Honda, O. Kitao, H. Nakai, T. Vreven, K. Throssell, J. A. Montgomery Jr., J. E. Peralta, F. Ogliaro, M. J. Bearpark, J. J. Heyd, E. N. Brothers, K. N. Kudin, V. N. Staroverov, T. A. Keith, R. Kobayashi, J. Normand, K. Raghavachari, A. P. Rendell, J. C. Burant, S. S. Iyengar, J. Tomasi, M. Cossi, J. M. Millam, M. Klene, C. Adamo, R. Cammi, J. W. Ochterski, R. L. Martin, K. Morokuma, O. Farkas, J. B. Foresman, D. J. Fox, Gaussian Inc, CT. Wallingford, **2016**.
[23] A. V. Marenich, C. J. Cramer, D. G. Truhlar, *J. Phys. Chem. B* **2009**, *113*, 6378–6396.
[24] a) S. Grimme, S. Ehrlich, L. Goerigk, *J. Comput. Chem.* **2011**, *32*, 1456–1465; b) S. Grimme, J. Antony, S. Ehrlich, H. Krieg, *J. Chem. Phys.* **2010**, *132*, 154104.
[25] a) A. D. Becke, *Phys. Rev. A* **1988**, *38*, 3098–3100; b) J. P. Perdew, *Phys. Rev. B* **1986**, *33*, 8822–8824; c) A. Schäfer, C. Huber, R. Ahlrichs, *J. Chem. Phys.* **1994**, *100*, 5829–5835; d) F. Weigend, R. Ahlrichs, *Phys. Chem. Chem. Phys.* **2005**, *7*, 3297–3305.
[26] H. S. Yu, X. He, S. L. Li, D. G. Truhlar, *Chem. Sci.* **2016**, *7*, 5032–5051.
[27] L. Goerigk, A. Hansen, C. Bauer, S. Ehrlich, A. Najibi, S. Grimme, *Phys. Chem. Chem. Phys.* **2017**, *19*, 32184–32215.
[28] G. Luchini, J. Alegre-Requena, I. Funes-Ardoiz, R. Paton, *F1000Research* **2020**, *9(Chem Inf Sci):291*, 1-14
[29] S. Grimme, *Chem. Eur. J.* **2012**, *18*, 9955–9964.

Version of record online: ■■, ■■

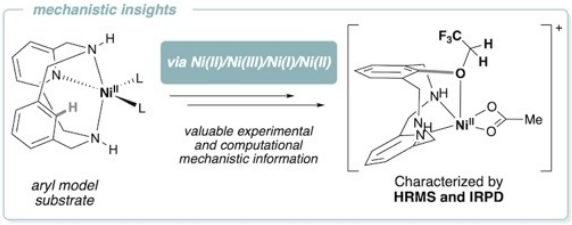

The trifluoro- and difluoroethoxylation of C(sp^2)-H bonds using nickel(II) complexes incorporating a model macrocyclic arene substrate is herein described. The stabilization properties of the model macrocyclic substrate allowed detecting and characterizing of the just-formed C(sp^2)-OCH_2CF_3-Ni(II) species by HRMS and He-tagging IRPD. The redox Ni(II)/Ni(III)/Ni(I) manifold constitutes valuable mechanistic information for the future design of new F-containing bioactive fluorinated aryl-alkyl ethers.

L. Capdevila, M. T. G. M. Derks, M. Montilla, J. M. Luis, J. Roithová*, X. Ribas**